


# An improved model of damage depth of shock-melted metal in microspall under triangular wave loading

Wen-Bin Liu(刘文斌), An-Min He(何安民), Kun Wang(王昆), Jian-Ting Xin(辛建婷), Jian-Li Shao(邵建立), Nan-Sheng Liu(刘难生), and Pei Wang(王裴)

**Citation:**Chin. Phys. B, 2021, 30 (**9**): 096202. DOI: 10.1088/1674-1056/abeb10
Journal homepage: http://cpb.iphy.ac.cn; http://iopscience.iop.org/cpb

**What follows is a list of articles you may be interested in**

---

## Reconstruction and interpretation of photon Doppler velocimetry spectrum for ejecta particles from shock-loaded sample in vacuum

Xiao-Feng Shi(石晓峰), Dong-Jun Ma(马东军), Song-lin Dang(党松琳), Zong-Qiang Ma(马宗强), Hai-Quan Sun(孙海权), An-Min He(何安民), and Pei Wang(王裴)
Chin. Phys. B, 2021, 30 (**6**): 066201. DOI: 10.1088/1674-1056/abd9b2

## Review on electrode-level fracture in lithium-ion batteries

Bo Lu(吕涛), Chengqiang Ning(宁成强), Dingxin Shi(史定鑫), Yanfei Zhao(赵炎翡), Junqian Zhang(张俊乾)
Chin. Phys. B, 2020, 29 (**2**): 026201. DOI: 10.1088/1674-1056/ab6841

## Ejecta from periodic grooved Sn surface under unsupported shocks

Wen-Bin Liu(刘文斌), Dong-Jun Ma(马东军), An-Min He(何安民), Pei Wang(王裴)
Chin. Phys. B, 2018, 27 (**1**): 016202. DOI: 10.1088/1674-1056/27/1/016202

## Influence of shockwave profile on ejecta from shocked Pb surface: Atomistic calculations

Guo-Wu Ren(任国武), Shi-Wen Zhang(张世文), Ren-Kai Hong(洪仁楷), Tie-Gang Tang(汤铁钢), Yong-Tao Chen(陈永涛)
Chin. Phys. B, 2016, 25 (**8**): 086202. DOI: 10.1088/1674-1056/25/8/086202

## Anti-plane problem analysis for icosahedral quasicrystals under shear loadings

Li Wu, Chai Yu-Zhen
Chin. Phys. B, 2014, 23 (**11**): 116201. DOI: 10.1088/1674-1056/23/11/116201

---

# An improved model of damage depth of shock-melted metal in microspall under triangular wave loading*

Wen-Bin Liu(刘文斌)[1,2,3], An-Min He(何安民)[2], Kun Wang(王昆)[4], Jian-Ting Xin(辛建婷)[5], Jian-Li Shao(邵建立)[6], Nan-Sheng Liu(刘难生)[1], and Pei Wang(王裴)[1,2,7,†]

[1] *Department of Modern Mechanics, University of Science and Technology of China, Hefei* 230027, *China*
[2] *Institute of Applied Physics and Computational Mathematics, Beijing* 100094, *China*
[3] *Graduate School of China Academy of Engineering Physics, Beijing* 100088, *China*
[4] *College of Materials Science and Engineering, Hunan University, Changsha* 410082, *China*
[5] *Science and Technology on Plasma Physics Laboratory, Research Center of Laser Fusion, China Academy of Engineering Physics, Mianyang* 621900, *China*
[6] *State Key Laboratory of Explosion Science and Technology, Beijing Institute of Technology, Beijing* 100081, *China*
[7] *Center for Applied Physics and Technology, Peking University, Beijing* 100871, *China*

(Received 6 December 2020; revised manuscript received 9 February 2021; accepted manuscript online 2 March 2021)

Damage depth is an important dynamic parameter for describing the degree of material damage and is also a key fundamental issue in the field of impact compression technology. The present work is dedicated to the damage depth of shock-melted metal in microspall under triangular wave loading, and an improved model of damage depth considering the material's compressibility and relative movement is proposed. The damage depth obtained from the proposed model is in good agreement with the laser-driven shock loading experiment. Compared with the previous model, the proposed model can predict the damage depth of shock-melted metal in microspall more accurately. Furthermore, two-groups of the smoothed particle hydrodynamics (SPH) simulations are carried out to investigate the effects of peak stress and decay length of the incident triangular wave on the damage depth, respectively. As the decay length increases, the damage depth increases linearly. As the peak stress increases, the damage depth increases nonlinearly, and the increase in damage depth gradually slows down. The results of the SPH simulations adequately reproduce the results of the proposed model in terms of the damage depth. Finally, it is found that the threshold stress criterion can reflect the macroscopic characteristics of microspall of melted metal.

**Keywords:** damage depth, theoretical modeling, microspall, triangular wave

**PACS:** 62.20.M−, 62.50.Ef, 62.20.mm **DOI:** 10.1088/1674-1056/abeb10

## 1. Introduction

When a triangular wave propagating in the material reflects from the free surface, the interaction of the incident rarefaction wave with the reflected rarefaction wave generates tensile stress that may internally damage the material, and this damage can range from small voids or cracks to macroscopic fractures and the ejection of one or several spall layers.[1] If the material is shocked above its melting pressure or melted on release from a lower shock pressure, tensile stress emerges in the melted materials and the dynamic damage process is referred to as "microspall".[2] Microspall has attracted great attention from scientists and engineers over the past decades because it has been observed in inertial confinement fusion[3–6] and laser-driven surface micromachining.[7–9]

Experimental, theoretical and computational studies of microspall have been carried out over the past decades. Andriot *et al.*[2] studied the effect of melting on spallation using Doppler laser interferometry and x-ray densitometry. Several features of microspall were reported, including a dramatic decrease in free-surface reflectivity, continuous ejection of material and a significant increase in the number of ejecta. Rességuier *et al.*[5,10] studied the microspall of tin using the time-resolved velocity measurements and post-shock observations of recovered targets and fragments, and they found that the velocity interferometer system for any reflector (VISAR) signal disappeared when the material melts, which is consistent with Andriot's discovery. Kanel *et al.*[11] investigated the spall strength of tin and lead, and they found that melting reduces the spall strength of lead and tin by at least an order of magnitude. Chen *et al.*[4] developed an improved Asay window technique to study the microspall of tin. An analytical method is developed to convert the measured data into the spatial volume density distribution, and the results are in good agreement with those obtained from x-ray radiograph. Theoretically, Kuksin *et al.*[12] established a spall model for liquids based on a void nucleation and growth approach. The model was applied to the estimation of liquid spall strength, and the result agrees well with experimental data. Xiang *et*

*Project supported by the National Natural Science Foundation of China (Grant Nos. U1530261 and 11572054) and the Science Challenge Project, China (Grant No. TZ2016001).

†Corresponding author. E-mail: wangpei@iapcm.ac.cn

© 2021 Chinese Physical Society and IOP Publishing Ltd 

*al*.[13] developed a model of microspall by coupling dynamic ductile damage and melting. The model was added to the finite element code and simulated spall experiments, and the simulation results are in good agreement with previous experiments. Computationally, molecular dynamics (MD) is an important theoretical tool for studying microspall. Luo *et al*.[14] investigated spallation in solid and liquid copper at high strain rates. Shao *et al*.[15,16] studied the failure mechanism and spall strength of single crystal aluminum under triangular wave loadings. Xiang *et al*.[17,18] studied the effects of shock intensity and loading rise time on the spall behavior of lead. Wang *et al*.[19] investigated the spall behaviors of melted lead under various triangular waves. However, most of the existing studies are focused on the mechanism of microspall damage, and there are few studies on the damage depth of microspall. Damage depth, the ratio of the damage mass per unit surface area to the density at rest condition, is an important parameter to describe the degree of damage. On the one hand, when a triangular wave reflects from the free surface of the material, the interaction of the incident rarefaction wave with the reflected rarefaction wave generates tensile stress that internally damages the material, where the material changes from continuous material to damaged material, and it is necessary to know the mass of damaged material. On the other hand, the damage depth is closely related to the physical processes such as secondary shock and particle-gas mixing.[20–22] Shao *et al*.[23] proposed an approximate description of damage depth under triangular wave loading when the material's compressibility is considered. However, under strong triangular wave loading, the effect of the relative movement is obvious and should also be taken into account when performing theoretical modeling of damage depth.

In order to study the damage depth of shock-melted metal in microspall under triangular wave loading, an improved model of damage depth of shock-melted metal is proposed, taking into account not only the effect of the material's compressibility, but also the effect of the relative movement. Then, the microspall is investigated in the laser-driven shock loading experiment, and the proposed model is compared with the experiment and the model considering only the effect of the material's compressibility.[23] Finally, the effects of peak stress and decay length of the incident triangular wave on the damage depth are investigated by SPH simulations. Besides, the applicability of the threshold stress criterion for melted metal at high strain rates is analyzed in microspall.

This paper is organized as follows. In Section 2, an improved model of damage depth of shock-melted metal in microspall is proposed. Then in Section 3, the proposed model is validated by the laser-driven shock loading experiment. In Section 4, the SPH simulations are carried out to investigate the effects of peak stress and decay length of the incident triangular wave on the damage depth. Finally, the conclusions are drawn in Section 5.

## 2. Proposed model

Under strong triangular wave loading, the material has already melted, and the effect of the material's compressibility is obvious. On the other hand, the effect of the relative movement is obvious in the time from the front of the incident triangular wave reaching the free surface of the material to the completion of last spallation. Therefore, using the threshold stress criterion and rules of propagation of simple wave, a model of damage depth of shock-melted metal in microspall is proposed considering the material's compressibility and relative movement.

When the incident triangular wave $I$ of peak stress $\sigma_{\mathrm{m}}$ and decay length $h_\lambda$ reflects from the free surface, the stress distribution near the free surface can be obtained on the assumption that the intensity of the reflected triangular wave $R$ remains constant, as shown in Fig. 1. The stresses of the incident triangular wave $I$ and reflected triangular wave $R$ inside the material at a distance $d$ from the free surface are $[(h_\lambda - 2d)/(h_\lambda)]\,\sigma_{\mathrm{m}}$ and $-\sigma_{\mathrm{m}}$, respectively, where the parameter $d$ represents the distance from the front of reflected triangular wave $R$ to the free surface. Therefore, the stress inside the material at a distance $d$ for the free surface is $(2d/h_\lambda)\sigma_{\mathrm{m}}$. Based on the threshold stress criterion, i.e., dynamic spallation occurs when the tensile stress reaches spall strength $\sigma_{\mathrm{s}}$, after the first spallation, the thickness of spall layer $d_1$ is given by

$$d_1 = \frac{\sigma_{\mathrm{s}}}{\sigma_{\mathrm{m}}}\frac{h_\lambda}{2}. \tag{1}$$

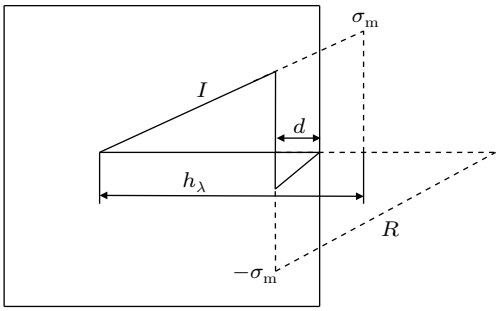



**Fig. 1.** Stress distribution near the free surface under triangular wave loading. The symbol $I$ represents the incident triangular wave, the symbol $R$ represents the reflected triangular wave, the quantities $\sigma_{\mathrm{m}}$ and $h_\lambda$ denote the peak stress and decay length of the incident triangular wave, respectively, and the quantity $d$ represents the distance from the front of reflected triangular wave $R$ to the free surface at the current moment.

For the remaining incident triangular wave inside the material, the peak stress is $\sigma_{\mathrm{m}} - \sigma_{\mathrm{s}}$ and the decay length is $h_\lambda - 2d_1$. If the peak stress of the incident triangular wave is high enough, the second spallation occurs, and the thickness of the spall layer remains constant. After the last spallation, the

number of spall layer $n$ and the failure depth of the material $h_{\rm d}$ are

$$n = \mathrm{INT}\left(\frac{\sigma_{\rm m}}{\sigma_{\rm s}}\right), \tag{2}$$

$$h_{\rm d} = n \cdot d_1 = \mathrm{INT}\left(\frac{\sigma_{\rm m}}{\sigma_{\rm s}}\right) \cdot \frac{\sigma_{\rm s}}{\sigma_{\rm m}} \frac{h_\lambda}{2}. \tag{3}$$

When the material is shocked above its melting pressure or melted on release from a lower shock pressure, the spall strength of melted material can be negligible compared with the peak stress, and the failure depth of the material $h_{\rm d}$ can be simplified as

$$h_{\rm d} \approx \frac{h_\lambda}{2}. \tag{4}$$

However, the failure depth $h_{\rm d}$ is independent of the material mass. Figure 2 gives a schematic diagram for solving the damage depth $h_{\rm s}$, which is defined as the ratio of the damage mass per unit surface area to the density at the rest condition. The main idea of solving the damage depth $h_{\rm s}$ is to know the failure depth $h_{\rm d}$ after the last spallation, and to solve the damage depth $h_{\rm s}$ at the moment when the front of the incident triangle wave reaches the free surface of the material, taking into account the effects of material's compressibility and relative movement. Therefore, damage material, the substance to the right of the blue dotted line at time $t_2$, is the substance to the right of the red dotted line at time $t_1$. According to the propagation laws of simple wave, the expression of the damage mass $m_{\rm s}$ and damage depth $h_{\rm s}$ induced by the ideal triangular wave in microspall can be derived as

$$m_{\rm s} = \frac{1}{2}\left(\rho_{\rm i} + \rho_{\rm m}\right)\left(h_{\rm d} + h_{\rm i}\right), \tag{5}$$

$$h_{\rm s} = \frac{m_{\rm s}}{\rho_0} = \frac{1}{2}\frac{\left(\rho_{\rm i} + \rho_{\rm m}\right)\left(h_{\rm d} + h_{\rm i}\right)}{\rho_0}, \tag{6}$$

where the $(1/2)\left(\rho_{\rm i} + \rho_{\rm m}\right)$ reflects the effect of material's compressibility, the $h_{\rm i}$ reflects the effect of relative movement, and $h_{\rm i}$, $\rho_{\rm m}$ and $\rho_{\rm i}$ are given by

$$\begin{aligned} h_{\rm i} &= \frac{u_{\rm m}}{8c_0 + 2u_{\rm m}} h_\lambda, \\ \rho_{\rm m} &= \frac{c_0 + s u_{\rm m}}{c_0 + (s-1)\,u_{\rm m}} \rho_0, \\ \rho_{\rm i} &= \left\{1 + \frac{2c_0 u_{\rm m}}{(4c_0 + u_{\rm m})\left[c_0 + (s-1)\,u_{\rm m}\right]}\right\} \rho_0. \end{aligned} \tag{7}$$

According to Eqs. (4), (6) and (7), if the material parameters ($\rho_0$, $c$, $s$), the peak velocity $u_{\rm m}$ (or peak stress $\sigma_{\rm m} = -\rho_0\left(c_0 + s u_{\rm m}\right) u_{\rm m}$) and decay length $h_\lambda$ of the incident triangular wave are known, the damage depth of the melted material $h_{\rm s}$ can be obtained under triangular wave loadings. The material parameters of tin are presented in Table 1.

**Table 1.** Material parameters of tin.

| $\rho_0$ (g/cm$^3$) | $c_0$ (km/s) | $s$ | $\gamma$ | $G_0$ (GPa) | $Y_0$ (GPa) |
|---|---|---|---|---|---|
| 7.287 | 2.59 | 1.49 | 2.27 | 21.0 | 0.16 |
| $Y_{\max}$ (GPa) | $\beta$ | $n$ | $G'_{\rm p}/G_0$ (GPa$^{-1}$) | $G'_{\rm T}/G_0$ (K$^{-1}$) | $T_{\rm m0}$ (K) |
| 0.30 | 130 | 0.1 | 0.088 | 0.0011 | 565 |

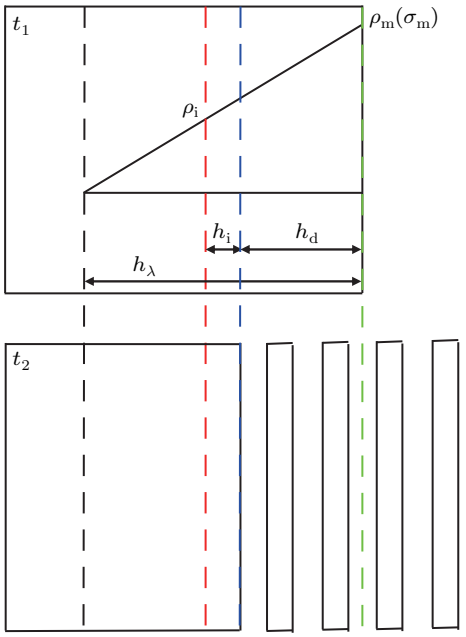



**Fig. 2.** Schematic diagram for solving the damage depth. $t_1$ is the moment when the incident triangular wave reaches the free surface, $t_2$ is the moment when the last spallation ends, the blue dotted line is the position of matrix at time $t_2$, the red dotted line is the position of blue dotted line at time $t_1$, the green dotted line is the beginning position of incident triangular wave and the black dotted line is the end position of incident triangular wave at time $t_1$. $\rho_{\rm i}$ is the density at the red dotted line at time $t_1$, the quantities $\rho_{\rm m}$, $\sigma_{\rm m}$ and $h_\lambda$ denote the peak density, peak stress and decay length of the incident triangular wave at time $t_1$, respectively, $h_{\rm d}$ is the failure depth, $h_{\rm i}$ is the relative movement between time $t_1$ and $t_2$.

## 3. Laser-driven experiment validation

After completing the theoretical model of the damage depth, the laser-driven experiments of microspall are performed. The damage depth obtained from the proposed model is compared with the experimental result and also compared with the model proposed by Shao *et al.*[23]

### 3.1. Experimental setup

The experiments are performed on the SGII-U laser facility. Figure 3 shows the experimental setup of microspall.[24] Two of eight driven laser beams work at 0.351 μm wavelength and with 3 ns duration, and focus onto the target at 45° angle. The beams are smoothed by the continuous phase plates (CPP), and the irradiated spots are quasi circular of about 2 mm diameter on the target.

The samples are tin foil with a thickness of 500 μm and a roughness of 400 nm after surface polishing. Two experiments

are performed on the tin sample with the same expected energy of the driving laser. The shot 1 is the microspall experiment, and the shot 2 adds a LiF window on the tin surface under the same conditions, which is used to measure the interface velocity history with photonic Doppler velocimetry (PDV) and obtain the profile of the incident triangular wave in the sample. The actual energy measured by the energy meter in shot 1 and shot 2 are 1282 J and 1272 J, respectively.

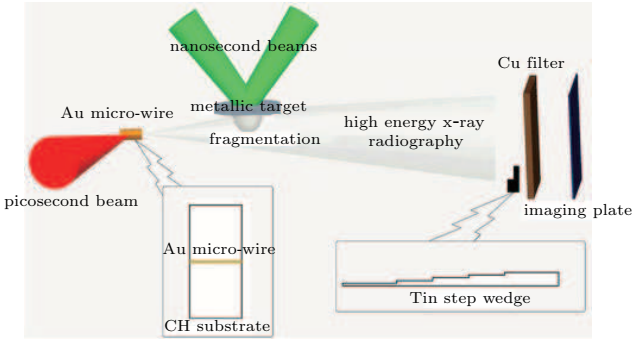



**Fig. 3.** The experimental setup of microspall.

### 3.2. Experimental results and analysis

Figure 4(a) shows the historical curve of the interface velocity between the tin sample and LiF in shot 2 based on PDV measurement. Since the incident shock wave is a triangular wave, the interface velocity continues to decay. The self-developed 2D SPH code[25,26] is used to determine the peak stress and decay length of the incident triangular wave. Therefore, the stress profile of the incident triangular wave in shot 1 and shot 2 can be determined, as shown in Fig. 4(b), where the peak stress is −36 GPa and the decay length is 198 μm. The historical curve of the interface velocity in SPH simulation is also shown in Fig. 4(a). Based on the initial maximum and early decreasing slope of the interface velocity, which determine the peak stress and unloading rate of the incident triangular wave, it can be seen that the SPH simulation is almost consistent with the experimental result.

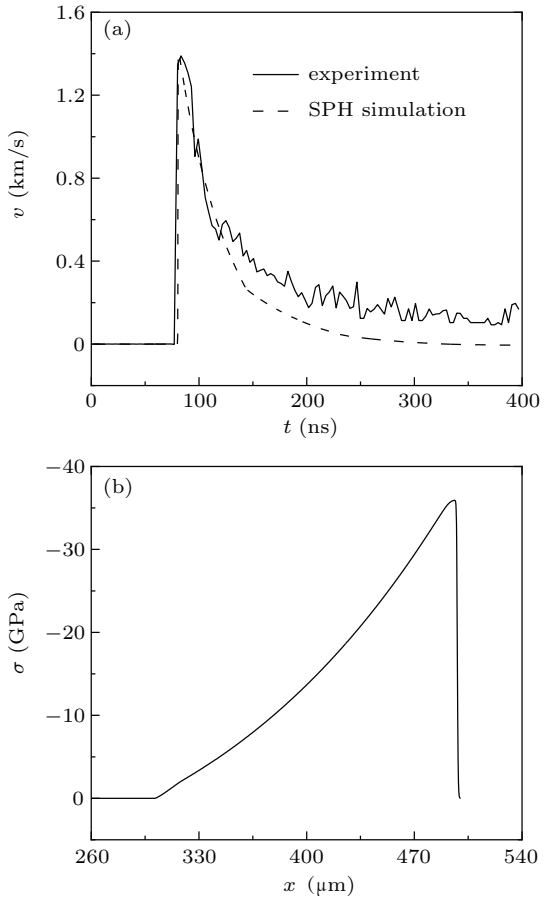



**Fig. 4.** (a) The historical curves of the interface velocity between the tin sample and LiF in shot 2 based on PDV measurement and SPH simulation. (b) Stress profile of the incident triangular wave from SPH simulation in shot 1 and shot 2.

**Table 2.** The damage depth obtained from the microspall experiment and models.

| Microspall experiment | The model considering only the material's compressibility[23] (relative error) | The proposed model considering both the material's compressibility and relative movement (relative error) |
|---|---|---|
| 142.9 μm | 125.9 μm (0.119) | 137.7 μm (0.036) |

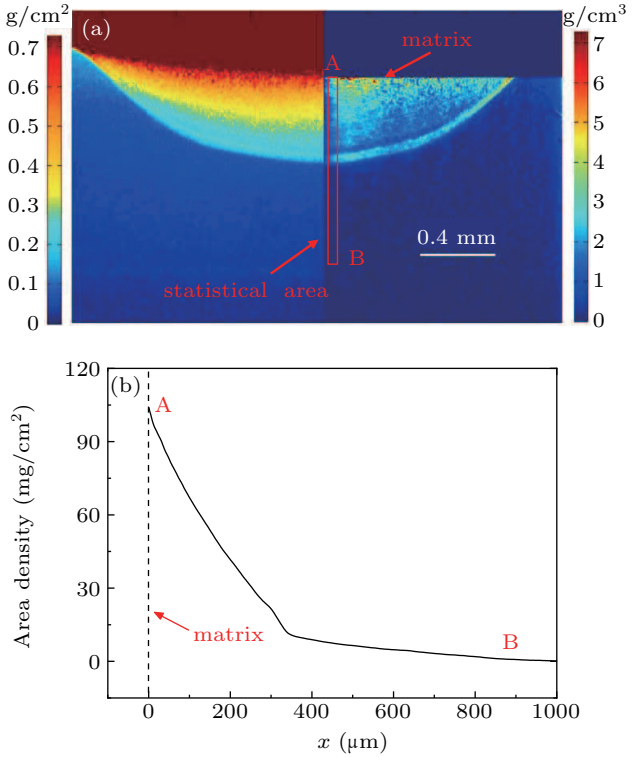



**Fig. 5.** (a) Areal density and volume density of the x-ray radiography image in shot 1. The red box is selected to count the volume density. (b) The areal density distribution along the shock direction. The symbol A indicates the position of matrix, and the symbol B indicates the start position of the statistics.

Figure 5(a) shows the areal density and volume density of the x-ray radiography image in shot 1, which are inferred from the step wedged. The central region along the impact direction is selected to count the volume density, as shown in the red box in the figure, and the width of the statistical region is 60 μm. Figure 5(b) shows the areal density distribution along

the impact direction. At the position of matrix, the areal density is 104.1 mg/cm$^2$, therefore, the damage depth $h_s = m_s/\rho_0$ can be obtained as 142.9 μm. Table 2 shows the damage depth obtained from the microspall experiment, the model considering only the material's compressibility[23] and the proposed model considering both the material's compressibility and relative movement. Since the effect of the relative movement is not considered, the damage depth of the model considering only the material's compressibility[23] is 125.9 μm with a relative error of 0.119. Compared with the model considering only the material's compressibility,[23] the damage depth of the proposed model considering both the material's compressibility and relative movement increases to 137.7 μm with a relative error of 0.036. It can be seen that the accuracy of the proposed model is improved as the effect of the relative movement is taken into account.

## 4. The effects of peak stress and decay length on the damage depth

According to the proposed model, it can be seen that, in addition to the material parameters, the peak stress and decay length of the incident triangular wave determine the damage depth. In this section, two-groups of SPH simulations are carried out to investigate the effects of peak stress and decay length on the damage depth, respectively, and the results of the SPH simulation are compared with the proposed model. In addition, the applicability of the threshold stress criterion for melted metals at high strain rates is analyzed in microspall.

### 4.1. Model and method

The microspall simulations of tin are carried out using a self-developed 2D SPH code.[25,26] In the SPH method, the material is discretized into a series of particles with independent information. Due to its Lagrangian nature, SPH has the advantage of simulating free-surface flows with large deformations.[27] The pressure is modeled by the Mie–Grüneisen equation of state,[28] as follows:

$$p = \left(1 - \frac{1}{2}\gamma\eta\right) p_{\mathrm{H}} + \gamma\rho e, \tag{8}$$

$$p_{\mathrm{H}} = \begin{cases} a_1\eta + a_2\eta^2 + a_3\eta^3, & (\eta \geq 0), \\ a_1\eta, & (\eta < 0), \end{cases} \tag{9}$$

where the $\eta = \rho/\rho_0 - 1$ is the compression ratio, $\gamma$ is the Grüneisen constant, and the parameters $a_1$, $a_2$, and $a_3$ are given by

$$\begin{aligned} a_1 &= \rho_0 c_0^2, \\ a_2 &= \rho_0 c_0^2 \left[1 + 2(s-1)\right], \\ a_3 &= \rho_0 c_0^2 \left[2(s-1) + 2(s-1)^2\right]. \end{aligned} \tag{10}$$

The Steinberg–Guinan constitutive model[29] is used, and the shear modulus strength $G$ and yield strength $Y$ are given as follows:

$$G = G_0 \left[1 + \frac{G'_p}{G_0}\frac{p}{\eta^{1/3}} - \frac{G'_T}{G_0}(T - 300)\right], \tag{11}$$

$$Y = Y_0 (1 + \beta\varepsilon^p)^n \left[1 + \frac{Y'_p}{Y_0}\frac{p}{\eta^{1/3}} - \frac{Y'_T}{Y_0}(T - 300)\right], \tag{12}$$

where the subscript "0" denotes the reference state ($T$ = 300 K, $p = 0$ Pa, $\varepsilon = 0$ s$^{-1}$), $\varepsilon^p$ is equivalent plastic strain, $\beta$ and $n$ are working hardening parameters, and $T$ is the temperature.

The melting temperature is modeled using the Lindermann's melting law[29]

$$T_{\mathrm{m}} = T_{\mathrm{m0}} \left(\frac{V_{\mathrm{m}}}{V_{\mathrm{m0}}}\right)^{2/3} \exp\left[2\frac{\gamma_0}{V_0}(V_{\mathrm{m0}} - V_{\mathrm{m}})\right], \tag{13}$$

where $T_{\mathrm{m0}}$ and $V_{\mathrm{m0}}$ are melting temperature and specific volume at reference state ($p = 0$ Pa, $\varepsilon = 0$ s$^{-1}$).

The threshold stress criterion is adopted, i.e., the tin spalls when the stress within the material is larger than $\sigma \geq \sigma_{\mathrm{min}} =$ 1.2 GPa. After tin melts, its spall strength is set to 0.1 GPa.[11] The material parameters of tin are presented in Table 1.

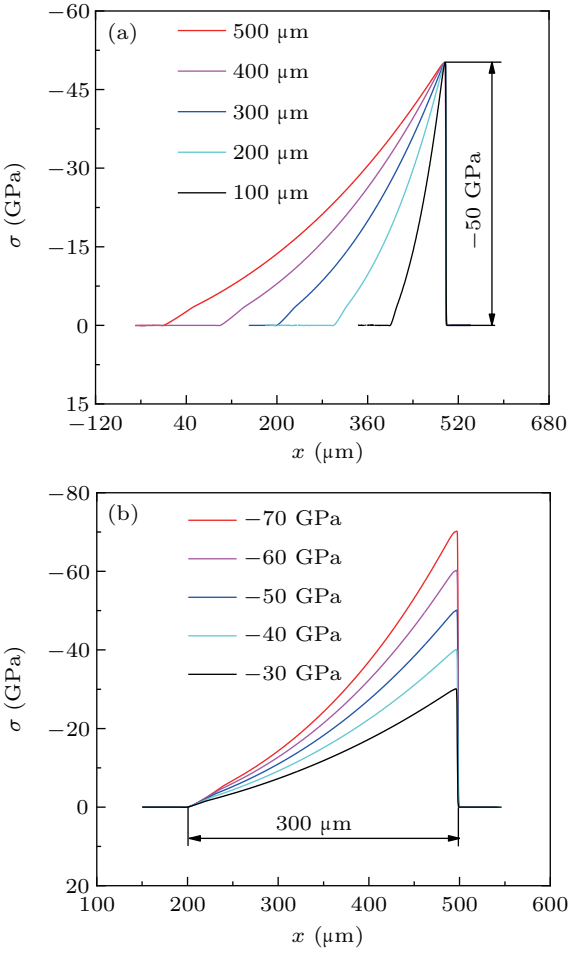



**Fig. 6.** The profiles of the incident triangular wave in SPH simulations: (a) different decay lengths at a peak stress of −50 GPa; (b) different peak stresses at a decay length of 300 μm.

In the simulation, the width of the sample is 100 μm, the initial inter-particle distance is 0.25 μm, and the smoothing length is 0.375 μm. Different triangular waves can be obtained by changing the length of sample, the length of flyer and the velocity of flyer. In the following discussion, the time is set to 0 ns when the front of the incident triangular wave reaches the free surface of sample. Two-groups of SPH simulations are conducted to investigate the effects of peak stress and decay length on the damage depth, respectively, and the profiles of the incident triangular waves are shown in Fig. 6. Figure 6(a) shows the profiles of the incident triangular waves when the peak stress is −50 GPa and the decay length is ranged from 100 μm to 500 μm, Figure 6(b) shows the profiles of the incident triangular waves when the decay length is 300 μm and the peak stress is ranged from −30 GPa to −70 GPa. The above peak stresses indicate that the tin has melted under the given loading conditions.[30]

### 4.2. SPH simulation results and analysis

Figure 7 gives the result of microspall at 300 ns when the peak stress is −50 GPa and the decay length is 300 μm. The black dotted line indicates the position of the matrix, so the material to the right of the black dotted line is the damage material in microspall, and the damage mass $m_s$ and damage depth $h_s = (m_s)/((1 \cdot l_y) \cdot \rho_0)$ can be obtained, where $l_y = 100$ μm is the width of the sample.

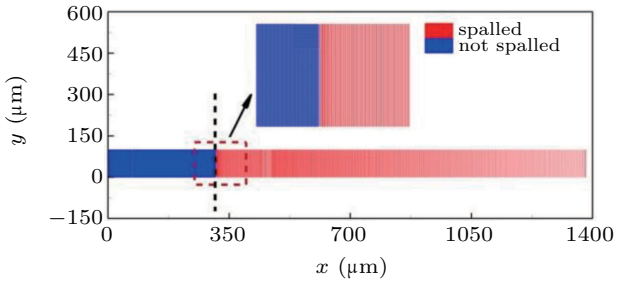



**Fig. 7.** Microspall at 300 ns in SPH simulations when the peak stress is −50 GPa, and the decay length is 300 μm. The black dotted line indicates the position of the matrix.

Figure 8 shows the results of the damage depth of the SPH simulations and the proposed model. As shown in Fig. 8(a), with the increase of decay length $h_\lambda$, the damage depth $h_s$ increases linearly, and the results of the SPH simulations agree well with those of the model with a maximum error of 0.029. As shown in Fig. 8(b), with the increase of peak stress $\sigma_m$, the damage depth $h_s$ increases nonlinearly, the increase in damage depth gradually slows down with an increase in peak stress $\sigma_m$, and the results of the SPH simulations agree well with those of the model with a maximum error of 0.033.

In contrast to the free-surface velocity associated with the first spallation, the damage depth is related to the spallation inside the material. Since the threshold stress criterion is adopted in the current SPH simulations, and the damage depths obtained from the SPH simulation are in good agreement with the results of the proposed model, it can be judged that the threshold stress criterion can satisfy the requirements of microspall of melted metal.

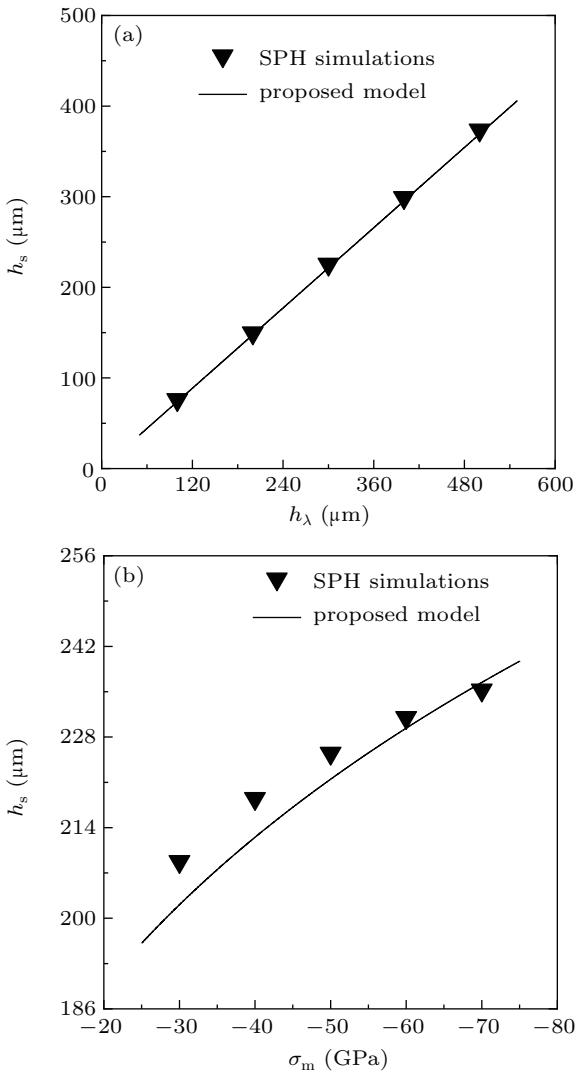



**Fig. 8.** The damage depth vs. (a) decay length $h_\lambda$ and (b) peak stress $\sigma_m$.

## 5. Conclusion

In this paper, an improved model of damage depth of shock-melted metal in microspall under triangular wave loading is proposed considering the material's compressibility and relative movement. Then, the microspall is investigated in the laser-driven shock loading experiment, and the damage depth obtained from the proposed model is compared with the experimental result. Finally, two-groups of SPH simulations are performed to investigate the effects of peak stress and decay length of the incident triangular wave on the damage depth. The details are as follows:

(I) Using the threshold stress criterion and rules of propagation of simple wave, a model of damage depth of shock-melted metal considering both the material's compressibility and relative movement is proposed. When the physical param-

eters of the material, peak velocity (or peak stress) and decay length of the triangular wave are known, the damage depth of the melted metal can be obtained under triangular wave loading. The proposed model is validated by the laser-driven experiment. Compared with the previous model, the proposed model can predict the damage depth of shock-melted metal in microspall more accurately.

(II) As the decay length increases, the damage depth increases linearly. As the peak stress increases, the damage depth increases nonlinearly, and the increase in damage depth gradually slows down. The results of the SPH simulation agree well with those of the proposed model.

(III) Combining the damage depth results of the SPH simulations and the proposed model, it is found that the threshold stress criterion can reflect the macroscopic characteristics of microspall of melted metal.

## References


[1] Antoun T, Seaman L, Curran D R, Kanel G I, Razorenov S V and Utkin A V 2003 *Spall Fracture* (New York: Springer) pp. 1–36

[2] Andriot P, Chapron P, Lambert V and Olive F 2004 *Shock Waves in Condensed Matter*, July 18–21, 1983, Amsterdam, North-Holland, p. 277280

[3] Smalyuk V A, Weber S V, Casey D T, Clark D S, Field J E, Haan S W, Hamza A V, Hoover D E, Landen O L, Nikroo A, Robey H F and Weber C R 2015 *High Power Laser Sci. Eng.* **3** E17

[4] Orth C D 2016 *Phys. Plasmas* **23** 022706

[5] Chen Y T, Hong R K, Chen H Y, Tang T G and Ren G W 2017 *Rev. Sci. Instrum.* **88** 013904

[6] Rességuier T D, Signor L, Dragon A and Roy G 2010 *Int. J. Fract.* **163** 109

[7] Dai Y, He M, Bian H D, Lu B, Yan X N and Ma G H 2012 *Appl. Phys. A* **106** 567574

[8] Oboňa J V, Ocelík V, Rao J C, Skolski J Z P, Römer G R B E, Huis in't Veld A J and Hosson J T M D 2014 *Appl. Surf. Sci.* **303** 118

[9] Shugaev M V, Shih C Y, Karim E T, Wu C and Zhigilei L V 2017 *Appl. Surf. Sci.* **417** 54

[10] Rességuier T D, Signor L, Dragon A, Boustie M, Roy G and Llorca F 2007 *J. Appl. Phys.* **101** 013506

[11] Kanel G I, Savinykh A S, Garkushin G V and Razorenov S V 2015 *J. Exp. Theor. Phys. Lett.* **102** 548

[12] Kuksin A Y, Norman G E, Pisarev V V, Stegailov V V and Yanilkin A V 2010 *Phys. Rev. B* **82** 174101

[13] Xiang M Z, Jiang S Q, Cui J Z, Xu Y and Chen J 2021 *Int. J. Plast.* **136** 102849

[14] Luo S N, An Q, Germann T C and Han L B 2009 *J. Appl. Phys.* **106** 013502

[15] Shao J L, Wang P, He A M, Duan S Q and Qin C S 2013 *J. Appl. Phys.* **113** 163507

[16] Shao J L, Wang P, He A M, Zhang R and Qin C S 2013 *J. Appl. Phys.* **114** 173501

[17] Xiang M Z, Hu H B, Chen J and Long Y 2013 *Model. Simul. Mater. Sci. Eng.* **21** 055005

[18] Xiang M Z, Chen J and Su R 2016 *Comput. Mater. Sci.* **173** 109421

[19] Wang K, Zhang F G, He A M and Wang P 2019 *J. Appl. Phys.* **125** 155107

[20] Shao J L, He A M and Wang P 2019 *Chin. J. High. Press. Phys.* **33** 030110 (in Chinese)

[21] Wang J N, Wu F C, Wang P, He A M and Wu H A 2020 *J. Appl. Phys.* **127** 135903

[22] Wu F C, Zhu Y B, Li X Z, Wang P, Wu Q and Wu H A 2019 *J. Appl. Phys.* **125** 185901

[23] Shao J L, Wang C, Wang P, He A M and Zhang F G 2019 *Mech. Mater.* **131** 78

[24] Chu G B, Xi T, Yu M H, Fan W, Zhao Y Q, Shui M, He W H, Zhang T K, Zhang B, Wu Y C, Zhou W M, Cao L F, Xin J T and Gu Y Q 2018 *Rev. Sci. Instrum.* **89** 115106

[25] Wang P, Shao J L and Qin C S 2009 *Acta. Phys. Sin.* **58** 1064 (in Chinese)

[26] Liu W B, Ma D J, He A M and Wang P 2018 *Chin. Phys. B* **27** 016202

[27] Liu M B and Zhang Z L 2019 *Sci. China Phys. Mech. Astron.* **62** 984701

[28] Jing F Q 1999 *Introduction to Experimental Equation of State* (Beijing: Science) pp. 25–29 (in Chinese)

[29] Tan H 2007 *Introduction to Experiemntal Shocked-Wave Physics* (Beijing: National Defence Inductry Press) pp. 113, 114, 188–190 (in Chinese)

[30] Monfared S K, Oró D M, Grover M, Hammerberg J E, LaLone B M, Pack C L, Schauer M M, Stevens G D, Stone J B, Turley W D and Buttler W T 2014 *J. Appl. Phys.* **116** 063504